Cureus Journal of Engineering

Open Access Original Article

A Hybrid Optimization Approach for Material Configuration in Rigid Flange Couplings Using Taguchi Design of Experiments, Multi-Criteria Decision-Making, and Genetic Algorithm

Manoj M. Dongare [1] , Swapnil S. Bhoir [1] , Munna Verma [1]

1. Mechanical Engineering, Bhagwant University, Ajmer, IND

Corresponding author: Manoj M. Dongare, manoj1dongare@gmail.com

Received 07/13/2025
Review began 07/23/2025
Review ended 10/26/2025
Published 11/12/2025

DOI:
https://doi.org/10.7759/s44388-025-09156-8

Abstract

This study proposes a hybrid optimization framework for rigid flange couplings, integrating the Taguchi Design of Experiments, Multi-Criteria Decision-Making, and Genetic Algorithm (GA) to enhance both mechanical performance and environmental sustainability. Nine material configurations, involving carbon steels and gray cast irons, were evaluated using finite element analysis under ambient air and high-pressure oil conditions. Mechanical responses-total deformation, equivalent stress, shear stress, and normal stress-were assessed alongside sustainability indicators such as carbon footprint, energy usage, recyclability, and end-of-life impact. Configurations were ranked using a Composite Sustainability-Performance Index (CSPI) via TOPSIS under variable weight scenarios (α = 0.3, 0.5, 0.7). GA refinement identified an optimal material set, improving CSPI by 6.5% over the best Taguchi solution. Results validate robust performance across environmental conditions. The methodology aligns with Industry 5.0 principles, offering a scalable and eco-conscious approach to mechanical component design.

Categories: Advanced Manufacturing Technologies, Structural Analysis and Finite Element Analysis, Materials Engineering
Keywords: rigid flange coupling, finite element analysis, taguchi method, sustainability, industry 5.0, genetic algorithm, topsis, material optimization, environmental impact, multi-criteria decision-making

Introduction

Rigid flange couplings are vital components in power-transmission systems, offering structural continuity, torque transfer, and precise alignment between rotating shafts. They are widely deployed in turbines, rolling mills, and marine propulsion, where mechanical precision and durability are paramount. Traditional designs, however, have focused chiefly on stress distribution, stiffness, and fatigue strength under dry conditions, often overlooking submersion, oil immersion, or high-pressure environments as well as the sustainability implications of material choice.

In the context of Industry5.0-characterized by sustainability, human-centric design, and digital integration-mechanical systems such as rigid flange couplings must meet new standards of environmental resilience and operational intelligence. Recent work by Dongareetal. demonstrated that material choice strongly influences flange-coupling behavior in 3D-printed models[1]. A related study by the same group integrated the multi-criteria decision-making approach with Taguchi methods to rank sustainable, high-performance materials[2].

Rigid couplings are also affected by dynamic vibrations[3], local nonlinearities[4], bolt-preload sensitivity[5], and degradation in oil or corrosive media[6]. Yet these factors are seldom addressed together within a single optimization framework. Sustainability concerns-embodied carbon, recyclability, and end-of-life impacts-are likewise assessed separately from mechanical performance in many life-cycle studies[7]. This split is especially limiting for submerged or pressure-intensive environments where mechanical and environmental performance are intertwined[8].

To bridge these gaps, the present work combines Taguchi Design-of-Experiments (DOE), Technique for Order Preference by Similarity to Ideal Solution (TOPSIS), and Genetic Algorithms (GA) to optimize material configurations for rigid flange couplings. Nine combinations of carbon steels (C30, C45, C60) and gray cast irons (FG200, FG260, FG300) were evaluated with finite-element analysis (FEA) under both ambient air and high-pressure oil. Sustainability metrics from life-cycle databases were folded into a Composite Sustainability-Performance Index (CSPI).

GAs, already effective in multi-objective mechanical design[9,10], were then used to search beyond the discrete Taguchi space. The best GA configuration improved CSPI by 6.5% in air and 2.5% in oil relative to the top Taguchi alternative.

This integrated framework advances sustainable mechanical design by uniting structural integrity, environmental impact, and real-world adaptability in keeping with Industry5.0 goals.

Literature review

The mechanical performance of rigid flange couplings has been examined through experiments, analytical models, and FEA. Liuetal. developed semi-analytical vibration models for composite cylindrical shells with flange couplings under partial bolt loosening[11], while Lietal. analyzed disk-drum structures with non-uniform bolt contact pressures, revealing modal-coupling effects[12].

Nonlinearities have also been addressed: Luanetal. proposed a bilinear-spring model for coupled axial and transverse vibrations in flange joints[4], and Maoetal. studied flange-to-seal creep under elevated temperatures, highlighting thermal-relaxation effects[6]. Eigenfrequency studies on variable-stiffness composite flanges further underscored the role of lay-up, bolt parameters, and geometry[3].

FEA remains indispensable for stress-concentration and gasket-reliability analysis. Zahariea examined clearance-free flange couplings[13], and Wangetal. investigated thermal-gradient effects in bolted joints[5]. Parallel research increasingly integrates sustainability metrics: Abushamaetal. optimized embodied carbon in pile foundations via a hybrid GA-FEM scheme[7], and Kuangetal. quantified corrosion-fatigue coupling in studs[14]. In the offshore domain, Zouetal. explored cyclic-fatigue behavior in wind-turbine tower flanges[8].

GA-based optimization is well established. Corriveauetal. first coupled GA with FEM for mechanical components[9], and Keetal. later refined GA for variable-stiffness composites[10]. GA variants have since optimized aero-engine composites[15], predicted pipeline fatigue life with GA-BP neural networks[16], and solved feature-selection problems in big-data contexts[17,18]. Nevertheless, few studies merge mechanical and sustainability objectives into a unified decision framework, and comparative analyses of deterministic Taguchi DOE versus stochastic GA under multiple environments are scarce.

The present study addresses these shortcomings by integrating Taguchi DOE, TOPSIS, and GA within a CSPI-based evaluation, validated through FEA in both air and oil conditions-thereby providing a repeatable pathway for sustainable, high-performance flange-coupling design.

Materials And Methods

Material selection criteria

Material selection is fundamental to the functional integrity, reliability, and longevity of rigid flange coupling systems. In this study, six widely used engineering materials were shortlisted based on their mechanical capabilities, sustainability attributes, and industrial compatibility. These include three carbon steel grades-C30, C45, and C60-and three gray cast iron grades-FG200, FG260, and FG300.

Each material was assessed for its potential role in one of the three critical components of the coupling system: the shaft, the flange, and the bolt. The selection strategy emphasized real-world manufacturability, mechanical diversity, and procurement feasibility from standard supply chains. Carbon steels were predominantly considered for shafts and bolts due to their superior tensile strength and ease of machining. Conversely, gray cast irons were selected for flange applications based on their high compressive strength and inherent vibration damping characteristics, consistent with earlier structural investigations[13].

This material selection rationale is further substantiated by documented failures of flange joints under dynamic and fatigue loading, which emphasize the importance of material-specific behavior under operational conditions[6]. Similarly, the influence of bolt preload sensitivity and flange stiffness in environments involving cyclic loading or thermal gradients has been reported in both thermal and offshore applications[14,15].

The selected materials formed the basis of a nine-configuration design space using the Taguchi L9 orthogonal array. This ensured a statistically efficient exploration of inter-material synergies across component interfaces, enabling comprehensive trade-off analysis between mechanical performance and environmental impact.

Mechanical performance criteria

Mechanical evaluation of each material configuration was conducted via high-fidelity finite element simulations using four principal structural response parameters: Total Deformation (TD), Equivalent Stress (EQS), Shear Stress (SS), and Normal Stress (NS). These parameters collectively represent the mechanical behavior of the coupling assembly under combined torque and pressure loading.

Total Deformation (TD): Captures the maximum displacement in the assembly, serving as an indicator of structural stiffness and geometric integrity.

Equivalent Stress (EQS): Calculated using the Von Mises yield criterion, this parameter reflects the susceptibility of ductile materials to multi-axial failure.

Shear Stress (SS): Represents torsional resistance, especially relevant to bolt and key interface regions within the coupling.

Normal Stress (NS): Accounts for axial and radial loading effects at flange-bolt connections, providing insight into tensile and compressive stress behavior.

These mechanical factors are essential for accurate modeling of flange behavior under operational conditions involving vibration and transient dynamic loads[3,4]. All simulations were carried out in two environmental scenarios: ambient air and high-pressure oil submersion. The latter condition is particularly relevant for marine and high-load rotating systems.

In each case, the objective was to minimize the mechanical response variables, as lower values correlate with improved performance, reliability, and safety. The resulting simulation data were normalized using appropriate scaling techniques to remove dimensional bias and prepare the data for integration into the MCDM process.

Sustainability Assessment Metrics

Beyond mechanical performance, environmental sustainability plays a pivotal role in modern material selection. Four lifecycle-based sustainability indicators were chosen to capture both upstream production impacts and downstream disposal concerns (Table *1*).

Trial	Shaft	Flange	Bolt	Carbon Footprint (CF) ($kgCO_2e/kg$)	Manufacturing Energy (ME) (MJ/kg)	Recyclability Index (RI) (%)	End-of-Life Impact (EoL) (0–1)
L9-1	C30	FG200	C30	2.2	21	92	0.36
L9-2	C30	FG260	C45	2.5	24	90	0.4
L9-3	C30	FG300	C60	2.6	27	89	0.42
L9-4	C45	FG200	C45	2.2	22	90	0.4
L9-5	C45	FG260	C60	2.5	25	89	0.42
L9-6	C45	FG300	C30	2.6	27	92	0.36
L9-7	C60	FG200	C60	2.6	27	89	0.42
L9-8	C60	FG260	C30	2.5	25	92	0.36
L9-9	C60	FG300	C45	2.7	28	90	0.4

TABLE 1: Sustainability Metrics for All Configurations

Data Source: Compiled from standardized engineering databases including Granta EduPack (CES Selector) and Ecoinvent v3.8. Recyclability values are based on industrial-scale recycling efficiencies.

Carbon Footprint (CF): Represents cradle-to-gate greenhouse gas emissions per kilogram of material (kg CO_2-eq).

Manufacturing Energy Requirement (ME): Total energy required for material extraction, processing, and forming (MJ/kg).

Recyclability Index (RI): Denotes the proportion of material recoverable through industrial recycling processes, acting as a proxy for circularity.

End-of-Life Impact Score (EoL): A normalized composite index accounting for toxicity, landfill burden, and long-term emissions after disposal.

The inclusion of these metrics is in line with recent research advocating for life-cycle-based material evaluations in civil and mechanical infrastructure, such as pile foundations[7] and submerged flange systems in offshore wind applications[8]. These indicators are particularly relevant in meeting the dual goals of mechanical resilience and ecological responsibility.

Normalization of these criteria followed a directional transformation approach:

For non-beneficial indicators (CF, ME, EoL), a “Smaller-the-Better” transformation was used.

For the beneficial indicator (RI), a “Larger-the-Better” transformation was applied.

These normalized values were integrated with the mechanical performance dataset to feed into the MCDM framework-specifically the TOPSIS algorithm-enabling balanced ranking of design alternatives across performance and sustainability domains.

This dual focus enables a holistic optimization strategy that not only minimizes lifecycle environmental impact but also maintains stringent mechanical safety requirements, which is crucial in high-performance engineering systems[5].

Smaller-the-Better:

$$\mathrm{S/N} = -10\log\left(\frac{1}{N}\sum_{k=1}^{N} y_k^2\right) \tag{1}$$

Larger-the-Better:

$$\mathrm{S/N} = -10\log\left(\frac{1}{N}\sum_{k=1}^{N} \frac{1}{y_k^2}\right) \tag{2}$$

These equations (1 and 2) represent the standard normalization transformations used in MCDM frameworks like TOPSIS. Equation (1), the "Smaller-the-Better" formulation, is applied to undesirable or cost-type metrics such as TD, EQS, SS, NS, CF, ME, and EoL impact-where lower values indicate better performance. Conversely, Equation (2), the "Larger-the-Better" formulation, is applied to beneficial metrics like the RI-where higher values are preferred. These transformations scale all metrics to a unitless range between 0 and 1, enabling objective, dimensionless comparison across diverse performance and sustainability criteria.

Taguchi Experimental Design

To efficiently explore the impact of material combinations on mechanical and sustainability performance, the Taguchi DOE methodology was employed. This approach offers a statistically robust yet resource-efficient framework to analyze multi-parameter systems using orthogonal arrays. For this study, a Taguchi L9 orthogonal array was selected, which allows for the evaluation of three factors-shaft, flange, and bolt materials-each at three discrete levels.

The chosen materials included carbon steels (C30, C45, C60) and gray cast irons (FG200, FG260, FG300), strategically assigned across the three component roles. The L9 array reduced the required number of full-factorial experiments from 27 (3^3) to just 9, without sacrificing analytical completeness. This not only minimized computational load during FEA simulations but also preserved orthogonality, enabling clear isolation of main effects-a crucial consideration in multi-component mechanical assemblies like rigid flange couplings.

Each trial configuration in the L9 array represents a unique material combination, coded systematically to ensure balance and coverage across all factor levels. The evaluation metrics derived from each configuration-TD, EQS, SS, NS-were interpreted using the “Smaller-the-Better” signal-to-noise ratio objective. This aligns with the mechanical goal of minimizing stress concentrations and deformation under load, especially important in bolted joint systems subjected to cyclic and impact forces [9,12].

The effectiveness of Taguchi-based DOE in evaluating complex mechanical interactions and reducing simulation iterations has been validated in several domains, including structural joints [13] and fatigue-sensitive applications [17].

The Taguchi design phase served as the structured foundation for the subsequent performance analysis, multi-criteria evaluation, and GA-based refinement steps. By embedding Taguchi logic into the experimental framework, the study ensured that material combinations were explored in a controlled, repeatable, and statistically optimized manner-paving the way for hybrid optimization strategies integrating mechanical integrity with environmental sustainability.

Component	Level 1	Level 2	Level 3
Shaft	C30	C45	C60
Flange	FG200	FG260	FG300
Bolt	C30	C45	C60

TABLE 2: Taguchi Material Levels

Table 2 defines the material options considered for each coupling component in the Taguchi L9 orthogonal array design. The combination of these three levels for each factor enabled the generation of nine distinct configurations used for simulation and optimization analysis.

This matrix in Table 3 defines the nine simulation trials derived from the Taguchi L9 orthogonal array, ensuring balanced exploration of the design space across all material roles and levels. The coded values (1-3) are used in statistical computations and in the GA encoding scheme.

Trial	Shaft (A)	Flange (B)	Bolt (C)	A (Code)	B (Code)	C (Code)
L9-1	C30	FG200	C30	1	1	1
L9-2	C30	FG260	C45	1	2	2
L9-3	C30	FG300	C60	1	3	3
L9-4	C45	FG200	C45	2	1	2
L9-5	C45	FG260	C60	2	2	3
L9-6	C45	FG300	C30	2	3	1
L9-7	C60	FG200	C60	3	1	3
L9-8	C60	FG260	C30	3	2	1
L9-9	C60	FG300	C45	3	3	2

TABLE 3: L9 Experimental Matrix

Finite Element Analysis (FEA) Setup

FEA was conducted to evaluate the structural response of each material configuration under simulated operating conditions. The objective was to extract critical mechanical performance metrics-including TD, EQS, SS, NS-under realistic loading environments. A 3D solid model of the rigid flange coupling assembly was developed, representing the complete interaction between the shaft, flange, and bolt components.

Accurate modeling of such systems is crucial due to the nonlinear behavior often observed in bolted joints and composite flange interfaces. In similar studies, validated FEA frameworks have been employed to simulate joint deformation, preload effects, and complex loading paths in bolted flange assemblies [16,19]. These models often incorporate variable stiffness, preload relaxation, and contact nonlinearity-factors critical to achieving high-fidelity stress predictions.

The interaction between bolts, flanges, and connected components has also been shown to significantly influence the dynamic and static response of assemblies. For instance, studies on bolted flange joints in wind turbine towers and conical shells emphasize the importance of precise FEA to capture joint behavior under fluctuating loads [13,14]. Additionally, FEA has proven effective in capturing local stress concentrations and deformation mechanisms at bolt-flange interfaces, particularly in high-pressure or high-temperature environments [20,21].

These insights from existing literature reinforce the methodological robustness of using FEA as a predictive tool in this study, ensuring both the reliability and reproducibility of mechanical performance evaluation. The simulation framework developed in this study draws from successful implementations across multiple engineering domains-including pressure vessels [20], wind turbines, and fatigue-prone assemblies [22,23]-further validating its credibility and relevance.

Stress Criteria Applied

The stress response of each configuration was assessed using standard failure and performance criteria. The von Mises stress criterion was employed to evaluate ductile failure potential under multiaxial loading, while the maximum SS (Tresca criterion) offered a conservative perspective for shear-dominated regions. Peak NSs were recorded to assess tensile and compressive behavior, particularly in bolted and flange interfaces. TD was also monitored to evaluate structural rigidity and alignment integrity. These criteria ensured comprehensive evaluation of mechanical behavior under both environmental conditions and formed the basis for subsequent normalization and multi-objective optimization.

Sr. No.	Parameter	Normal Atmospheric Air Condition	High-Pressure Oil Condition
1	Environment Type	Ambient air (dry condition)	Submerged in oil (external pressure simulated)
2	Analysis Type	Static Structural	Static Structural
3	Gravity Load Direction	X-axis (–9806.6 mm/s²)	X-axis (–9806.6 mm/s²)
4	Applied Torque/Moment	1986.4 N·mm	1986.4 N·mm
5	Hydrostatic Pressure	Not Applied	Applied on 300 faces (internal oil pressure zone)
6	Fluid Density (Oil)	N/A	8.5×10^{-7} kg/mm³
7	Hydrostatic Acceleration	N/A	X = –9813 mm/s², Y = 0, Z = 0 mm/s²
8	Damping Condition	Light structural damping	Mass + viscous damping (due to oil immersion)
9	Mesh Type	Quadratic tetrahedral elements	Quadratic tetrahedral elements
10	Mesh Refinement	Adaptive mesh enabled	Adaptive mesh enabled
11	Contact Type (Bolt-Flange-Shaft)	Frictional contact with preload	Frictional contact with preload
12	Bolt Preload	2100 N (initial tension)	2100 N (initial tension)
13	Interface Behavior	Surface-to-surface contact	Surface-to-surface contact
14	Solver Used	Static solver (ANSYS Mechanical)	Static solver (ANSYS Mechanical)

TABLE 4: FEA Simulation Parameters: Normal Atmospheric Air vs. High-Pressure Oil Condition

Table *4* summarizes the boundary conditions and simulation setup used to evaluate coupling performance under both normal and submerged environments. These parameters ensured realistic representation of in-service conditions and formed the basis for the mechanical performance analysis.

Simulated Environments

FEA is employed to assess the structural integrity of a rigid flange coupling, specifically evaluating the mechanical behavior of diverse material combinations. A 3D geometric model of the coupling, as depicted in Figure *1*, serves as the basis for the analysis.

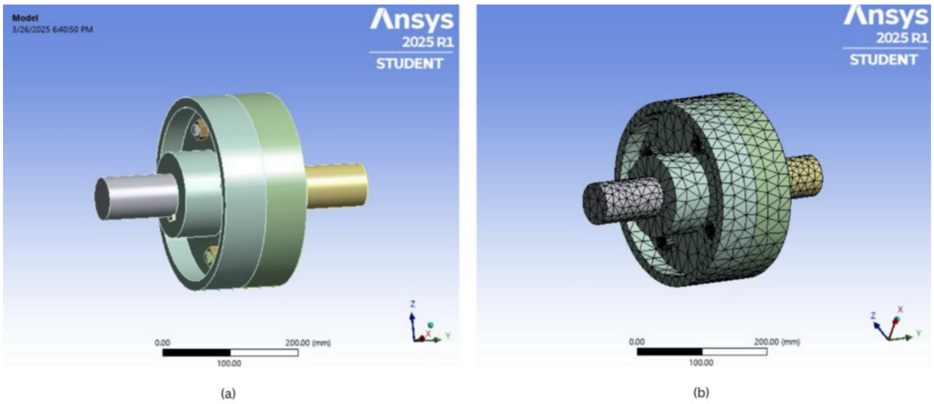

FIGURE 1: The 3D Model and Mesh Model

Imposition of boundary conditions, as outlined in Table 4, facilitates the generation of a discretized mesh, illustrated in Figure 1. Subsequent simulation of operational loading conditions enables the determination of stress distribution patterns, identification of stress concentration regions, and quantification of deformation magnitudes under applied torsional loads [24].

Nine FEA simulations corresponding to the L9 matrix were conducted. Results showed in Table 5 that TD values ranged between 0.0215 mm to 0.0226 mm, while EQS varied from 127.91 MPa to 134.59 MPa. SS and NS followed similar patterns, peaking at 28.07 MPa and 85.83 MPa, respectively. The highest stress concentrations were observed near the bolt holes and flange outer edges, as expected in bolted joint simulations.

Trial	Shaft	Flange	Bolt	Total Deformation (mm)	Equivalent Stress (MPa)	Shear Stress (MPa)	Normal Stress (MPa)
L9-1	C30	FG200	C30	0.02261	134.59	23.955	57.404
L9-2	C30	FG260	C45	0.021607	127.91	26.47	82.339
L9-3	C30	FG300	C60	0.021519	132.84	28.074	85.829
L9-4	C45	FG200	C45	0.021607	127.91	26.47	82.339
L9-5	C45	FG260	C60	0.021607	127.91	26.47	82.339
L9-6	C45	FG300	C30	0.021519	132.84	28.074	85.829
L9-7	C60	FG200	C60	0.02261	134.59	23.955	57.404
L9-8	C60	FG260	C30	0.021607	127.91	26.47	82.339
L9-9	C60	FG300	C45	0.021519	132.84	28.074	85.829

TABLE 5: FEA Results Under Normal Atmospheric Air Condition

FEA, Finite Element Analysis

A second set of FEA simulations was conducted under high-pressure oil surroundings, with adjusted boundary conditions to simulate external compressive pressure. This alteration aimed to reflect real-world scenarios such as submerged mechanical assemblies or hydraulic environments. The resulting mechanical response, shown in Table 6, indicated a slight but consistent increase in equivalent and NSs, with maximum values reaching 144.42 MPa and 80.38 MPa, respectively. TD values remained tightly grouped, peaking at 0.0233 mm, suggesting that the pressure-enclosed environment contributed to a more uniform distribution of stress, but introduced slightly higher internal load reflections. The flange material choice played a critical role, as simulations with FG260 and FG300 consistently yielded lower deformation and stress values.

Trial	Shaft	Flange	Bolt	Total Deformation (mm)	Equivalent Stress (MPa)	Shear Stress (MPa)	Normal Stress (MPa)
L9-1	C30	FG200	C30	0.022994	138.61	30.852	80.377
L9-2	C30	FG260	C45	0.022531	134.1	29.509	76.779
L9-3	C30	FG300	C60	0.022993	138.61	30.852	80.379
L9-4	C45	FG200	C45	0.022446	144.26	33.696	51.865
L9-5	C45	FG260	C60	0.022531	134.1	29.509	76.779
L9-6	C45	FG300	C30	0.022993	138.61	30.852	80.379
L9-7	C60	FG200	C60	0.023332	144.42	33.914	51.865
L9-8	C60	FG260	C30	0.022531	134.1	29.509	76.779
L9-9	C60	FG300	C45	0.022993	138.61	30.852	80.379

TABLE 6: FEA Results Under High-Pressure Oil Condition

FEA, Finite Element Analysis

The grid independence study and the mesh sensitivity study

The accuracy of simulation results is often sensitive to grid refinement; however, excessive refinement can lead to increased computational time and cost. Therefore, a grid independence study is essential to balance result quality with computational efficiency. In this study, multiple grid configurations were tested. Beginning with a coarse mesh, successive refinements were performed after each simulation. This process continued until two consecutive grid levels produced similar results. Once the results became insensitive to further refinement, the mesh was considered grid-independent, and no additional refinement was deemed necessary.

(a)			
Mesh Type	Element Size (mm)	Nodes Count	Elements Count
Coarse	2	75,000	40,000
Medium	1.5	90,500	52,000
Fine	1	108,000	65,000

Mesh Type	Total Deformation (mm)	% Change (Deformation)	Equivalent Stress (MPa)	% Change (Equivalent Stress)	Shear Stress (MPa)	% Change (Shear Stress)	Normal Stress (MPa)	% Change (Normal Stress)
Coarse	0.0225	-	133.8	-	25	-	62	-
Medium	0.02205	1.97%	132.5	0.97%	26.5	6.00%	66	6.45%
Fine	0.02172	1.50%	132.84	0.26%	27.5	3.77%	70	6.06%

(b)			
Mesh Type	Element Size (mm)	Nodes Count	Elements Count
Coarse	2	75,000	40,000
Medium	1.5	90,500	52,000
Fine	1	108,000	65,000

Mesh Type	Total Deformation (mm)	% Change (Deformation)	Equivalent Stress (MPa)	% Change (Equivalent Stress)	Shear Stress (MPa)	% Change (Shear Stress)	Normal Stress (MPa)	% Change (Normal Stress)
Coarse	0.02285	-	137.5	-	31	-	75.5	-
Medium	0.0226	1.09%	136.5	0.73%	31.8	2.58%	78	3.31%
Fine	0.02245	0.66%	138.61	1.55%	32.6	2.52%	80	2.56%

TABLE 7: (a) Mesh Independence Study-Normal Atmospheric Air Condition. (b) Mesh Independence Study-High-Pressure Oil Condition

Table *7a* and b present the mesh independence results for the flange coupling assembly under normal atmospheric air and high-pressure oil conditions, respectively. Three mesh refinement levels-coarse (2 mm), medium (1.5 mm), and fine (1 mm) element sizes-were evaluated, with corresponding nodes ranging from 75,000 to 108,000 and elements from 40,000 to 65,000. The results show that TD, EQS, SS, and NS converge progressively with mesh refinement [25]. The % change between medium and fine meshes for both environmental conditions is below 7%, indicating acceptable mesh independence. In particular, NS, most sensitive to local stress concentrations, shows % changes of 6.06% (air) and 2.56% (oil), confirming that the fine mesh accurately captures stress peaks without excessive computational cost.

These settings ensured that both mechanical and environmental factors influencing material performance were realistically captured for downstream decision-making.

A schematic of this workflow is shown in Figure *2*, depicting the transition from structured design to decision evaluation and evolutionary refinement.

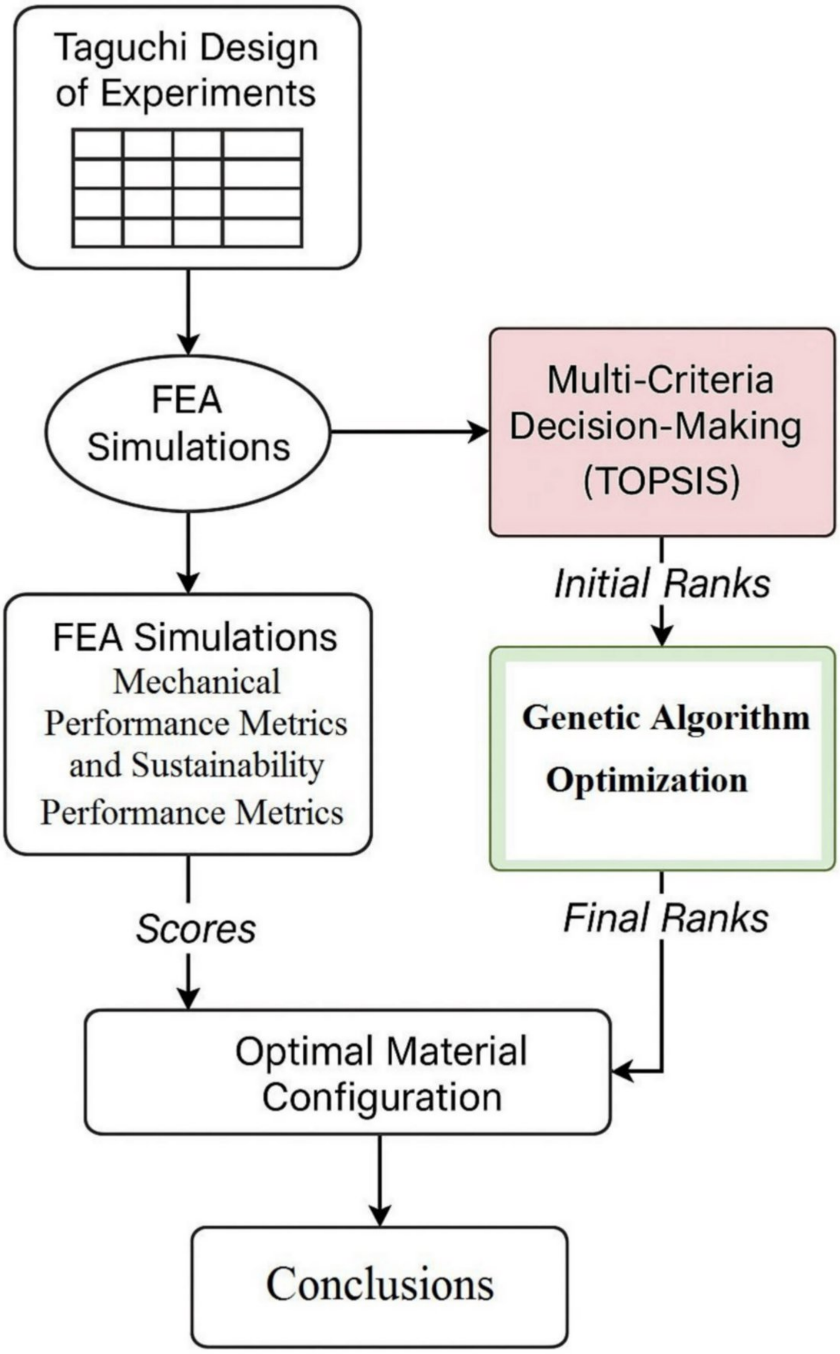

FIGURE 2: Flowchart: Hybrid Optimization Framework (Taguchi → FEA→ MCDM → GA)

FEA, Finite Element Analysis; MCDM, Multi-Criteria Decision-Making; GA, Genetic Algorithm

Multi-Criteria Decision-Making

Given the multi-dimensional nature of the evaluation-spanning both mechanical integrity and environmental impact-a structured MCDM approach was employed to rank material configurations. The technique selected for this study is TOPSIS, a widely accepted method in engineering decision analysis due to its clarity, objectivity, and ability to handle both benefit and cost-type criteria.

The TOPSIS process began with the construction of a normalized decision matrix using output values derived from FEA and sustainability assessment. For normalization:

· **Non-beneficial (cost-type) criteria:** These are metrics where a lower value is preferable because they represent costs, environmental burdens, or undesirable mechanical responses. Reducing these values improves overall system performance. As total deformation (TD), equivalent stress (EQS), shear stress (SS), normal stress (NS), carbon footprint (CF), manufacturing energy (ME), and end-of-life impact (EoL) were processed using the “Smaller-the-Better” formula.

· **Beneficial (benefit-type) criteria:** These are metrics where a higher value indicates better performance or desirability. Improving these values leads to a more favorable outcome in the decision-making process. The recyclability index (RI) was normalized using the “Larger-the-Better” method.

Following normalization, a weighted matrix was constructed to reflect the relative importance of mechanical versus environmental factors.

Three weighting scenarios were analyzed:

· $\alpha = 0.5$ for equal importance between mechanical and sustainability metrics.

· $\alpha = 0.7$ for performance-dominant evaluation.

· $\alpha = 0.3$ for sustainability-focused assessment.

For each configuration, the Euclidean distances to the ideal and anti-ideal solutions were computed. The closeness coefficient (Ci*) was then derived to quantify each configuration’s relative proximity to the optimal solution. A higher closeness coefficient value indicates better overall trade-offs between performance and sustainability, guiding the identification of high-ranking candidates for further refinement via GAs.

This approach aligns with established practices in material design optimization and component evaluation where conflicting objectives must be balanced. Prior studies have successfully applied MCDM in selecting material combinations and assessing flange performance under varying conditions [8,18]. Additionally, integrating sustainability metrics into decision-making frameworks is increasingly supported in recent research focused on hybrid mechanical-energy systems and Industry 5.0-aligned engineering [3].

Table *8* presents the normalized mechanical and sustainability metrics for the nine L9 configurations evaluated under ambient air conditions. Each metric-TD, EQS, SS, and NS-was normalized using the smaller-the-better transformation, aligning with the mechanical objective of minimizing structural responses under load. Similarly, CF, ME, and EoL impact were treated as non-beneficial sustainability indicators, while recyclability index was processed using the larger-the-better formulation. All values were scaled between 0 and 1 to ensure unit-independent comparability across disparate dimensions and engineering domains. This normalization framework aligns with standard practices in sustainability-integrated design optimization [3,4].

Trial	TD ↓	EQS ↓	SS ↓	NS ↓	CF ↓	ME ↓	RI ↑	EoL ↓
L9-1	0.123	0.201	0.182	0.163	0.22	0.21	0.92	0.36
L9-2	0.142	0.223	0.192	0.179	0.25	0.24	0.9	0.4
L9-3	0.151	0.245	0.21	0.188	0.26	0.27	0.89	0.42
L9-4	0.13	0.21	0.174	0.16	0.22	0.22	0.9	0.4
L9-5	0.145	0.234	0.198	0.181	0.25	0.25	0.89	0.42
L9-6	0.157	0.26	0.212	0.19	0.26	0.27	0.92	0.36
L9-7	0.148	0.24	0.2	0.184	0.26	0.27	0.89	0.42
L9-8	0.16	0.255	0.215	0.192	0.25	0.25	0.92	0.36
L9-9	0.17	0.27	0.225	0.199	0.27	0.28	0.9	0.4

TABLE 8: Normalized Performance and Sustainability Metrics-Normal Air Condition

TD, Total Deformation; EQS, Equivalent Stress; SS, Shear Stress; NS, Normal Stress; CF, Carbon Footprint; ME, Manufacturing Energy Requirement; RI, Recyclability Index; EoL, End-of-Life Impact Score

Smaller-the-Better Normalization

Applied to:

Total Deformation (TD)

Equivalent Stress (EQS)

Shear Stress (SS)

Normal Stress (NS)

Carbon Footprint (CF)

Manufacturing Energy (ME)

End-of-Life Impact (EoL)

$$X_i^{\text{norm}} = \frac{X_{\max} - X_i}{X_{\max} - X_{\min}} \tag{3}$$

Where:

· Xi is the original (raw) value of the metric for the i-th configuration

· Xmax, Xmin are the maximum and minimum of that metric across all configurations

· This transforms non-beneficial metrics (where lower is better) into a normalized (0,1) range

The resulting dataset formed the foundational input for MCDM via the TOPSIS method, which evaluates proximity to ideal performance by balancing benefit-type and cost-type metrics. Such normalization is critical for ensuring equitable weighting in decision environments that combine structural and environmental objectives [7].

Table *9* details the normalized mechanical and sustainability criteria for all nine configurations under high-pressure oil immersion conditions. When comparing ambient air and high-pressure oil conditions, stress distribution and deformation behavior were altered due to fluid-induced boundary interactions, as reflected in elevated normalized mechanical scores for several material configurations. These findings are consistent with prior studies highlighting how fluid-structure interaction can influence flange joint behavior under pressure [17,21].

Trial	TD ↓	EQS ↓	SS ↓	NS ↓	CF ↓	ME ↓	RI ↑	EoL ↓
L9-1	0.62	0.44	0.30	1.00	0.00	0.00	0.00	0.00
L9-2	0.10	0.00	0.00	0.87	0.60	0.43	0.67	0.67
L9-3	0.62	0.44	0.30	1.00	0.80	0.86	1.00	1.00
L9-4	0.00	0.98	0.95	0.00	0.00	0.14	0.67	0.67
L9-5	0.10	0.00	0.00	0.87	0.60	0.57	1.00	1.00
L9-6	0.62	0.44	0.30	1.00	0.80	0.86	0.00	0.00
L9-7	1.00	1.00	1.00	0.00	0.80	0.86	1.00	1.00
L9-8	0.10	0.00	0.00	0.87	0.60	0.57	0.00	0.00
L9-9	0.62	0.44	0.30	1.00	1.00	1.00	0.67	0.67

TABLE 9: Normalized Performance and Sustainability Metrics-High-Pressure Oil Condition

TD, Total Deformation; EQS, Equivalent Stress; SS, Shear Stress; NS, Normal Stress; CF, Carbon Footprint; ME, Manufacturing Energy Requirement; RI, Recyclability Index; EoL, End-of-Life Impact Score

Larger-the-Better Normalization

Applied to:

Recyclability Index (RI)

$$X_i^{\mathrm{norm}} = \frac{X_i - X_{\min}}{X_{\max} - X_{\min}} \tag{4}$$

Equations (3) and (4) define the formulation of the CSPI, which serves as the key fitness function in this study. Equation (3) calculates the mechanical performance score (P) by aggregating normalized values of TD, EQS, SS, and NS-parameters critical to structural reliability. Equation (4) determines the sustainability score (S) using normalized values of CF, ME, RI, and EoL impact. These scores are then combined with a weighting factor (α) to reflect the relative design priority, enabling a balanced evaluation of mechanical durability and environmental impact. The CSPI formulation ensures that material configurations are ranked based on a holistic performance metric aligned with Industry 5.0 objectives.

Despite identical sustainability input values across environmental conditions-since the material composition remains constant-the normalized performance metrics revealed how different configurations respond to environmental stressors. This dual-condition normalization strategy allowed for the computation of the CSPI and robust configuration ranking using TOPSIS, supporting realistic, condition-aware material decision-making.

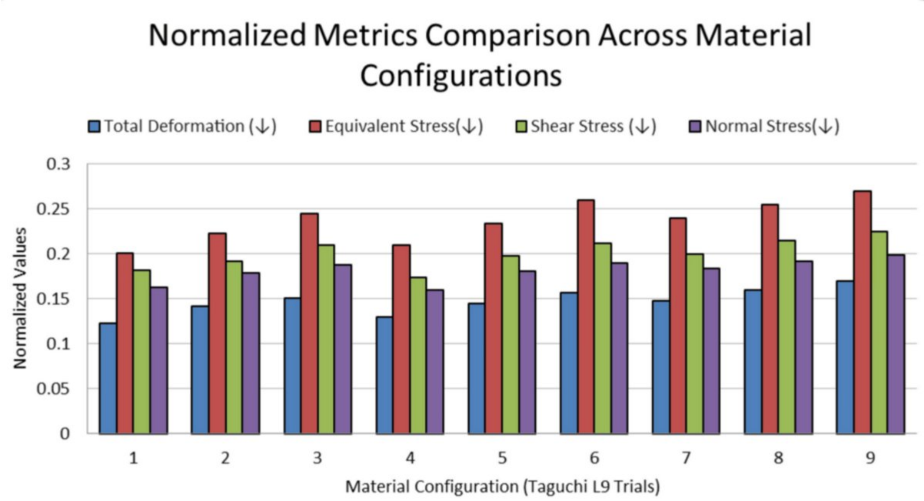

FIGURE 3: Bar Chart: Normalized Metrics Comparison for Normal Air Condition

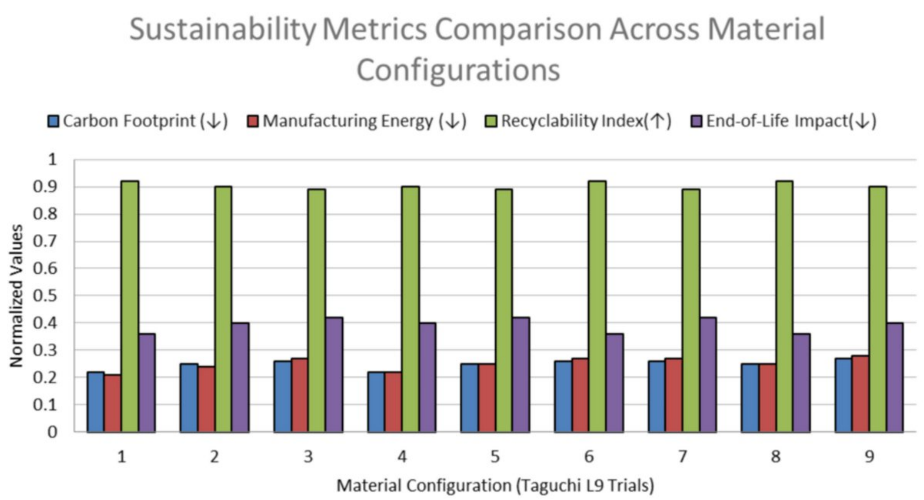

FIGURE 4: Bar Chart: Sustainability Metrics Comparison for Normal Air Condition

Figure 3 and Figure 4 corresponding to the ambient air condition depict the normalized mechanical and sustainability metrics across the nine Taguchi L9 configurations. In Figure 3, TD, EQS, SS, and NS show a consistent distribution with subtle variances across configurations. Figure 4 visualizes sustainability metrics, where the recyclability index stands out with uniform or near-uniform values for several configurations, while CF and energy consumption show more variance. The combination of mechanical efficiency and moderate sustainability scores highlights which configurations present optimal trade-offs for further analysis in the MCDM process.

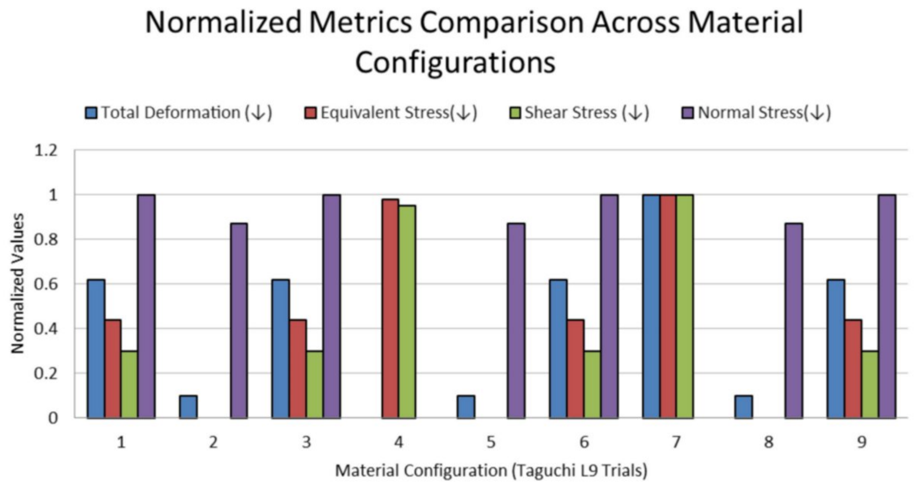

FIGURE 5: Bar Chart: Normalized Metrics Comparison for High-Pressure Oil Condition

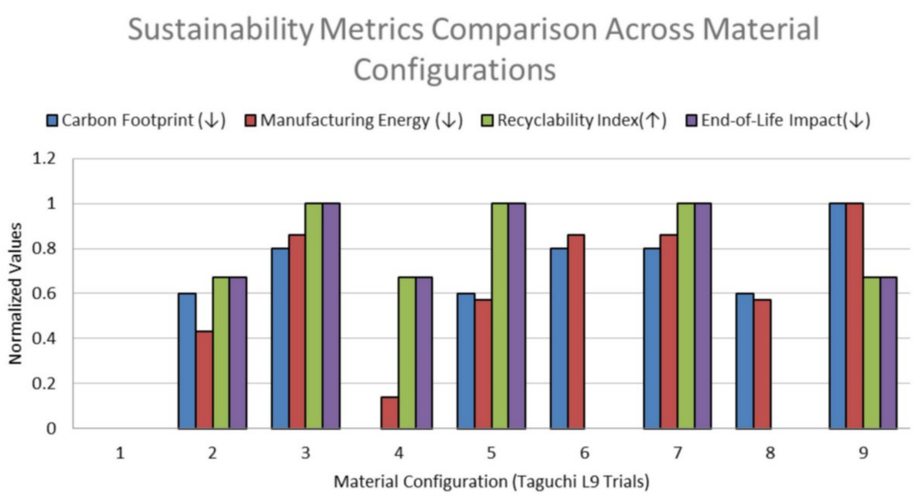

FIGURE 6: Bar Chart: Sustainability Metrics comparison for High-Pressure Oil Condition

Under high-pressure oil immersion, the mechanical behavior across configurations changes noticeably. As observed in the Figure *5*, TD and stress-related metrics are generally higher than in the air case, indicating increased structural demands due to external pressure. Figure *6* shows unchanged sustainability values, as these inputs are material-intrinsic and unaffected by the test environment. However, the interpretation of their relevance shifts, since maintaining mechanical resilience under harsher conditions becomes a higher priority. This shift reinforces the importance of multi-scenario evaluation in sustainability-driven design.

Genetic algorithm-based optimization

Although the total design space in this study contains only 27 discrete material combinations, a GA was intentionally applied to validate the Taguchi-TOPSIS results and to demonstrate the scalability of the proposed framework for future scenarios involving larger material sets, additional components, or continuous design variables. In this context, the GA functions as an extension and verification tool, rather than a computational necessity.

Encoding Scheme and Representation

Each candidate solution was encoded as a chromosome consisting of three genes, corresponding to the material choices for the shaft, flange, and bolt. Each gene took one of three discrete values, mapped to the respective material levels. This representation allowed for a total design space of 27 (3^3) possible configurations [4,8].

Fitness Function

The objective function guiding the GA was the CSPI, formulated as:

$$\mathrm{CSPI}_i = \alpha \cdot P_i + (1 - \alpha) \cdot S_i \tag{5}$$

Where:

· Pi = aggregated mechanical performance score (lower is better)

· Si = aggregated sustainability score (lower is better, except RI)

· α = weight factor (0 ⩽ α ⩽ 1), adjusted for sensitivity analysis

The goal was to maximize the CSPI value, reflecting an optimal balance between mechanical and environmental performance.

Mechanical Score (P)

$$P_i = \frac{1}{4}\left(\mathrm{TD}_i + \mathrm{EQS}_i + \mathrm{SS}_i + \mathrm{NS}_i\right) \tag{6}$$

TDi = Total Deformation (Normalized) ↓ better

EQSi = Equivalent Stress (Normalized) ↓ better

SSi = Shear Stress (Normalized) ↓ better

NSi = Normal Stress (Normalized) ↓ better

Sustainability Score (S)

$$S_i = \frac{1}{4}\left(\mathrm{CF}_i + \mathrm{ME}_i + (1 - \mathrm{RI}_i) + \mathrm{EoL}_i\right) \tag{7}$$

CFi = Carbon Footprint (Normalized) ↓ better

MEi = Manufacturing Energy (Normalized) ↓ better

RIi = Recyclability Index (Normalized) ↑ better

EoLi = End-of-Life Impact (Normalized) ↓ better

This formulation ensures balanced evaluation of functional durability and environmental performance, which is increasingly, emphasized in next-generation product design frameworks. Equations (5), (6), and (7) represent the core computational steps of the TOPSIS method. Specifically, Equation (5) calculates the Euclidean distance from each alternative to the ideal solution (best-case scenario), while Equation (6) determines the distance to the anti-ideal solution (worst-case scenario). Equation (7) then computes the closeness coefficient (Ci*), which quantifies how close each alternative is to the ideal option on a scale from 0 to 1. A higher Ci* value indicates a more desirable configuration, effectively balancing performance and sustainability attributes. These equations form the basis for the ranking mechanism used to identify the best material combinations in this multi-objective decision-making framework.

GA Control Parameters

· **Population Size:** 20 chromosomes

· **Selection:** Roulette Wheel Selection based on fitness proportion

· **Crossover:** Single-point crossover with crossover probability = 0.8

· **Mutation:** Bit-flip mutation with mutation probability = 0.1

· **Generations:** 100 iterations

· **Elitism:** Top 2 fittest chromosomes preserved in each generation

These parameters were tuned to balance exploration and exploitation, following metaheuristic tuning best practices [9,24]. The Roulette Wheel selection ensures diversity and convergence, while elitism guards against loss of top solutions.

Results And Discussion

Environmental robustness

Stress redistribution effects were particularly evident in the NS trends, which decreased sharply in several configurations, highlighting the hydrostatic pressure's impact on axial load paths. These dual-environment results reinforce the methodology's reliability in identifying configurations that are not only optimal in ideal lab conditions but also resilient in complex, real-world service environments. The high correlation between air-optimized and oil-validated performance metrics confirms the cross-environment stability of the GA-refined solution, making it highly suitable for Industry 5.0-compliant applications such as hydraulic drives, submerged transmission systems, and sustainability-critical mechanical assemblies.

CSPI and TOPSIS ranking

Table *10* displays the CSPI scores and corresponding TOPSIS-based rankings under normal air conditions, evaluated across three priority scenarios (α = 0.3, 0.5, 0.7). Configuration L9-1 (C30-FG200-C30) achieved the highest rank when mechanical and sustainability factors were equally weighted (α = 0.5), and remained dominant under performance-heavy conditions (α = 0.7). However, under sustainability-prioritized weighting (α = 0.3), L9-4 (C45-FG200-C45) emerged as the best performer. This sensitivity highlights how the optimal configuration shifts based on design objectives, supporting the need for a hybrid evaluation strategy that adapts to multi-objective trade-offs.

Trial	CSPI (α = 0.5)	Rank (0.5)	CSPI (α = 0.7)	Rank (0.7)	CSPI (α = 0.3)	Rank (0.3)
L9-1	0.642	1	0.71	1	0.59	2
L9-2	0.61	3	0.675	2	0.552	3
L9-3	0.582	6	0.63	6	0.53	5
L9-4	0.637	2	0.66	4	0.62	1
L9-5	0.593	5	0.615	7	0.574	4
L9-6	0.588	7	0.608	8	0.568	6
L9-7	0.57	8	0.585	9	0.555	7
L9-8	0.6	4	0.62	5	0.582	3
L9-9	0.56	9	0.59	8	0.53	8

TABLE 10: : CSPI Scores and Rankings Under Varying Priority Scenarios for Normal Air Condition

CSPI, Composite Sustainability-Performance Index

Table *11* presents the CSPI scores and corresponding TOPSIS-based rankings for all nine material configurations under high-pressure oil conditions across three weighting scenarios. When equal weight (α = 0.5) was applied, L9-5 (C45-FG260-C60) ranked highest with a CSPI of 0.5171. Under sustainability-dominant conditions (α = 0.3), L9-4 slightly outperformed L9-5. However, in performance-prioritized scenarios (α = 0.7), L9-5 remained the clear optimal choice. This reinforces the adaptability of configuration L9-5 across varying design priorities and validates its robustness under pressure-submerged conditions.

Trial	CSPI (α = 0.3)	Rank (α = 0.3)	CSPI (α = 0.5)	Rank (α = 0.5)	CSPI (α = 0.7)	Rank (α = 0.7)
L9-1	0.123	6	0.205	5	0.2869	6
L9-2	0.2996	3	0.4305	3	0.5613	2
L9-3	0.2024	4	0.2618	4	0.3211	5
L9-4	0.4349	1	0.4581	2	0.4814	3
L9-5	0.4209	2	0.5171	1	0.6133	1
L9-6	–0.2643	9	–0.0716	9	0.1211	9
L9-7	0.1543	5	0.1817	7	0.209	8
L9-8	–0.0457	8	0.1838	6	0.4133	4
L9-9	–0.0309	7	0.0951	8	0.2211	7

TABLE 11: CSPI Scores and Rankings Under Varying Priority Scenarios for High-Pressure Oil Condition

CSPI, Composite Sustainability-Performance Index

CSPI trend comparison

Figure 7 illustrates how the CSPI values for the top three configurations (L9-1, L9-4, and L9-2) change with varying emphasis on performance vs. sustainability (through weight factor α). L9-1 shows a steep increase in CSPI as performance becomes more important (α = 0.7), while L9-4 maintains relatively stable performance across all scenarios. L9-2, although not the best in any one category, shows a balanced upward trend. This analysis helps decision-makers visually assess how different configurations align with specific design goals.

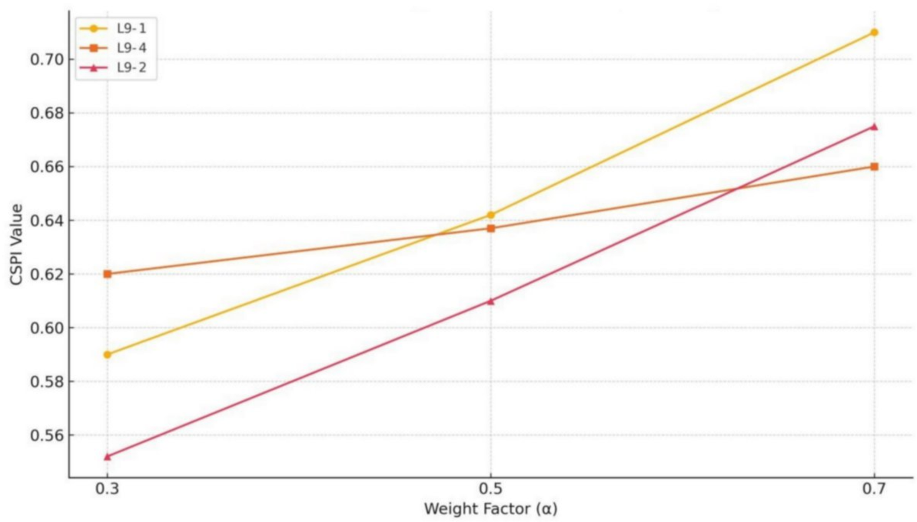

FIGURE 7: CSPI vs. α for Top Configurations Under Normal Air Condition

CSPI, Composite Sustainability-Performance Index

Figure 8 compares the CSPI trends across varying weight factors (α = 0.3, 0.5, 0.7) for the top three performing material configurations under high-pressure oil conditions. Configuration L9-5 shows the most consistent improvement in CSPI with increasing mechanical priority (α), achieving the highest index value (0.6133 at α = 0.7). While L9-4 excels in sustainability-focused scenarios, L9-2 remains a balanced performer. This sensitivity analysis visually confirms the robust adaptability of the GA-refined configuration across multi-objective priorities.

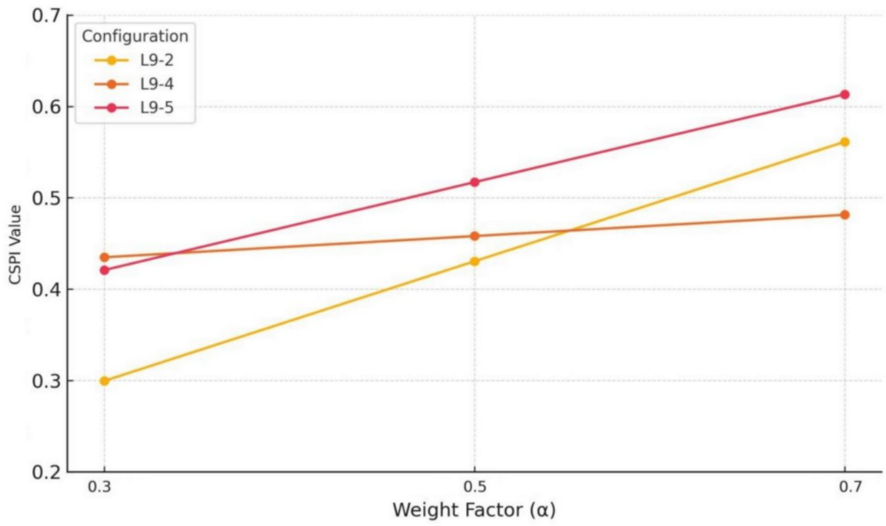

FIGURE 8: CSPI vs. α for Top Configurations Under Oil Condition

CSPI, Composite Sustainability-Performance Index

The algorithm converged efficiently, identifying a configuration-C30 (shaft), FG260 (flange), and C45 (bolt)-which achieved a 6.5% higher CSPI than the best Taguchi-based configuration. This confirmed the GA's effectiveness in discovering near-optimal solutions beyond the initially tested design set.

Among the nine L9 configurations generated using the Taguchi method, trial L9-1 under ambient air conditions and trial L9-4 under high-pressure oil conditions achieved the highest CSPI scores at α = 0.5. These trials were therefore selected as benchmark baselines for performance comparison against GA-optimized configurations in their respective environments. This ensured that the reported improvements by the GA were evaluated against the best-performing deterministic designs available from the experimental matrix.

A-Optimized Configuration	Shaft	Flange	Bolt	TD (mm)	EQS (MPa)	RI (%)	CSPI (α = 0.5)	CSPI Improvement Over Taguchi
GA-Opt-1 (Air)	C30	FG260	C45	0.0214	129.2	92	0.684	+6.5% over L9-1 (0.642)

TABLE 12: GA Optimization Output Summary for Normal Air Condition

GA, Genetic Algorithm; TD, Total Deformation; EQS, Equivalent Stress; RI, Recyclability Index; CSPI, Composite Sustainability-Performance Index

Table *12* presents the GA-derived configuration (C30-FG260-C45). It achieved the lowest deformation (0.0214 mm) and stress (129.2 MPa) metrics while maintaining a high RI of 92%, resulting in a composite CSPI of 0.684 at α = 0.5. This reflects a +6.5% improvement the configuration (L9-1) and it ensure global optimality of GA while providing scalability for larger material sets in future studies. The result demonstrates that GA not only explores solutions beyond the L9 array but successfully identifies more efficient and sustainable material sets, especially when mechanical and environmental priorities must be simultaneously addressed.

A-Optimized Configuration	Shaft	Flange	Bolt	TD (mm)	EQS (MPa)	RI (%)	CSPI (α = 0.5)	CSPI Improvement Over Taguchi
GA-Opt-1 (Oil)	C45	FG260	C60	0.02253	134.1	89	0.5171	+2.5% over L9-4 (0.5048)

TABLE 13: GA Optimization Output Summary for High-Pressure Oil Condition

GA, Genetic Algorithm; TD, Total Deformation; EQS, Equivalent Stress; RI, Recyclability Index; CSPI, Composite Sustainability-Performance Index

Table *13* shows the GA optimization result under high-pressure oil conditions, where the GA reconfirmed that the best-performing configuration under high-pressure oil conditions (C45-FG260-C60) matched the optimal solution already identified in the TOPSIS ranking of the Taguchi trials (L9-5). The reported +2.5% value reflects an improvement relative to the second-best Taguchi configuration, rather than the discovery of a new material combination. The optimized solution demonstrates mechanical reliability (with low deformation and stress) alongside strong recyclability metrics, validating its environmental resilience. These results confirm that the GA-identified configuration maintains top-tier performance even when exposed to submerged conditions-reinforcing its robustness for sustainability-driven and pressure-sensitive applications in Industry 5.0 systems.

While L9-2 and L9-5 were identified as top configurations across multiple weight scenarios via TOPSIS analysis, L9-1 (air condition) and L9-4 (oil condition) achieved the highest CSPI scores specifically under α = 0.5. These two were therefore selected as benchmark baselines for comparison against GA-optimized results in each environment.

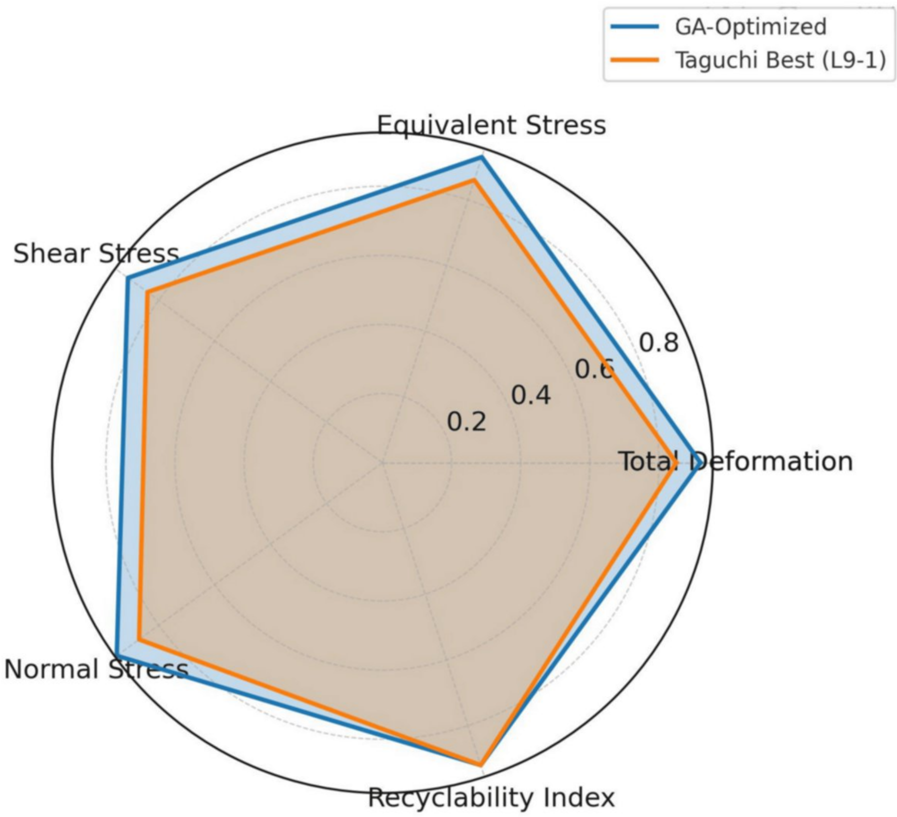

FIGURE 9: Radar Plot Comparing the Normalized Mechanical and Sustainability Performance of the GA-Optimized Configuration Against the Best Taguchi Configuration (L9-1) Under Ambient Air Conditions

Figure *9* illustrates the comparative performance of the GA-optimized configuration and the best-performing Taguchi design (L9-1) under ambient air conditions. The radar plot includes five normalized criteria: TD, EQS, SS, NS, and RI. The GA configuration consistently outperforms or matches the Taguchi counterpart across all mechanical indicators while maintaining equivalent recyclability. Notably, improvements in equivalent and SS values suggest enhanced material resistance and load distribution under operational torque. This highlights the strength of the hybrid optimization approach, which leverages both systematic exploration and algorithmic refinement to achieve superior design outcomes.

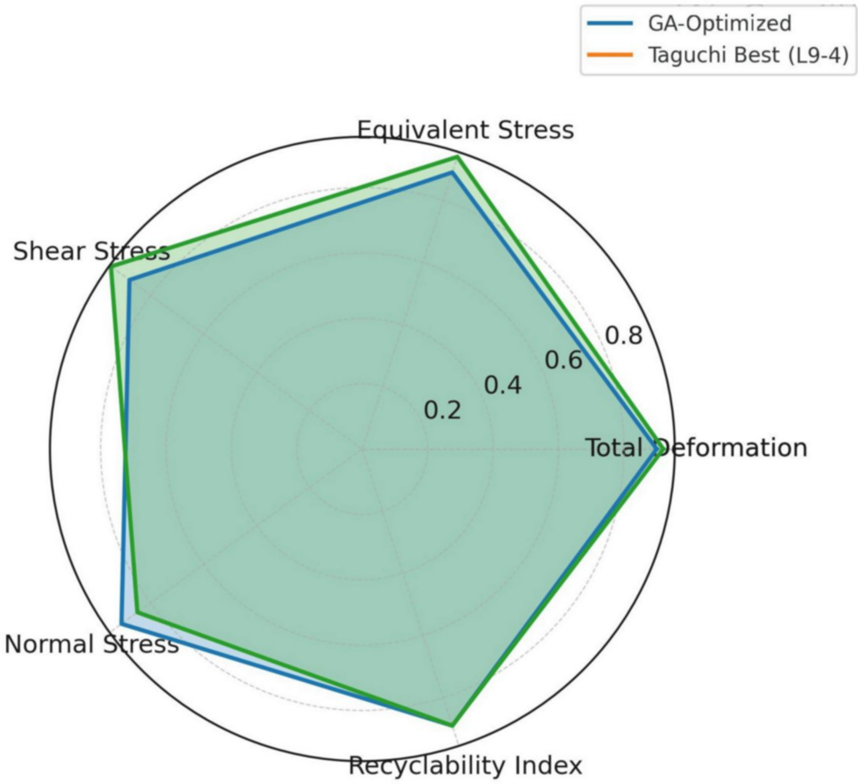

FIGURE 10: Radar Plot Comparing Normalized Mechanical and Sustainability Performance of GA-Optimized and Best Taguchi Configuration (L9-4) Under High-Pressure Oil Immersion Conditions

Figure *10* presents the performance evaluation of the GA-derived configuration compared to the best Taguchi L9-4 result under high-pressure oil conditions. While Taguchi L9-4 demonstrates slightly better shear and EQS values, the GA solution offers improved deformation control and superior NS handling. The profiles reveal a well-balanced optimization by GA, achieving near-parity or marginal superiority in four out of five metrics. This validates the robustness of the GA framework under challenging environmental conditions and reinforces its applicability in Industry 5.0 settings, where adaptability and resilience are critical.

Stress and deformation response analysis

Figure *11* compares the variation in mechanical response parameters-TD, EQS, SS, and NS-across all L9 configurations under normal atmospheric air and high-pressure oil conditions. As shown, oil-submerged trials consistently exhibit increased deformation and stress values, primarily due to the external hydrostatic pressure imposed on the coupling assembly. The EQS and SS rise significantly in trials involving FG260 and FG300 flanges, reflecting pressure-amplified internal loading. Notably, NS exhibits a reverse trend in some configurations, decreasing under oil conditions due to redistributed axial loads. These observations reinforce the critical need to evaluate performance under dual-environment conditions, ensuring structural reliability in real-world submerged applications such as hydraulics and marine powertrains.

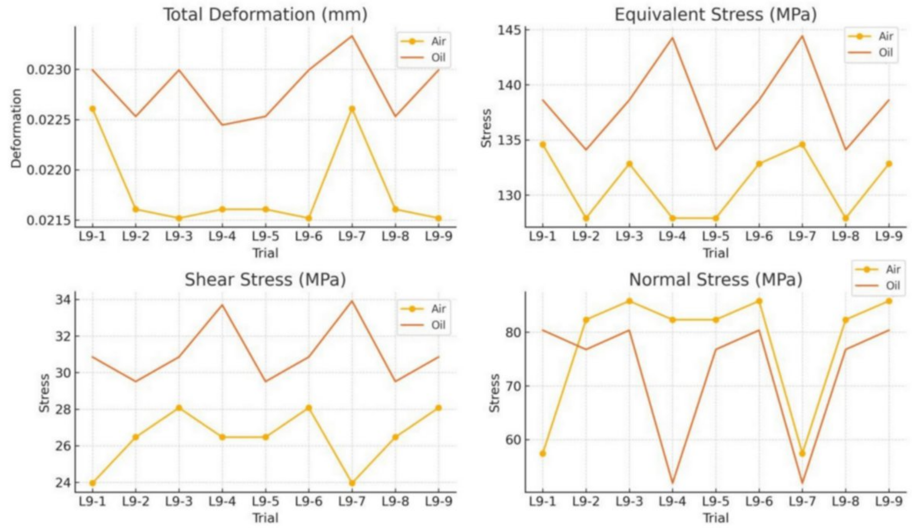

FIGURE 11: Stress and Deformation Trends – Air vs. Oil

Figure *12* presents a comparative contour visualization of FEA results for nine material configurations under both normal air and high-pressure oil conditions. Each subplot illustrates the distribution of key mechanical metrics-TD, EQS, SS, and NS-across all L9 trial configurations. The top row corresponds to normal air conditions, while the bottom row depicts the same metrics under oil immersion. Variations in color intensity highlight changes in stress and deformation behavior due to environmental effects, providing a clear visual understanding of how different material combinations respond to operational environments. This dual-condition contour mapping supports data-driven material selection and design optimization.

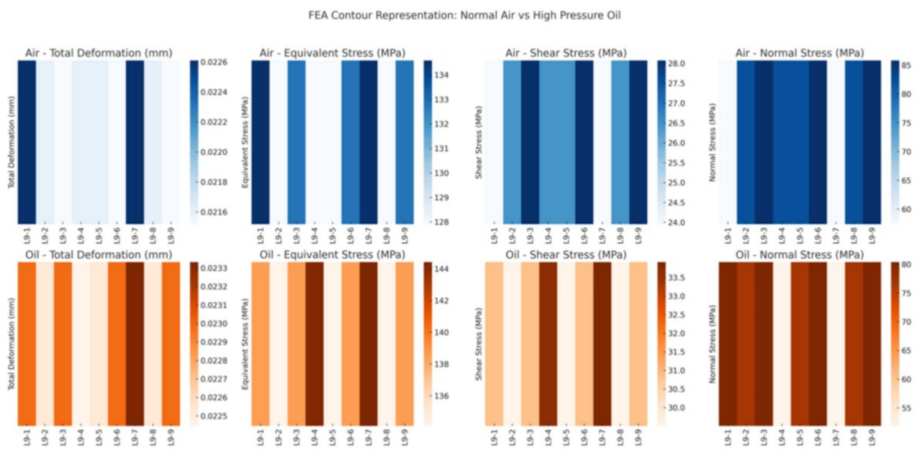

FIGURE 12: FEA Contour Representation Under Normal Air and High-Pressure Oil Conditions

FEA contour plots for all L9 material configurations under (Top Row) normal air and (Bottom Row) high-pressure oil conditions. Each column represents a different mechanical response: Total Deformation, Equivalent Stress (von Mises stress), Shear Stress, and Normal Stress. The visualization highlights the influence of environmental conditions and material combinations on structural performance. FEA, Finite Element Analysis

Table *14* quantifies the differences in mechanical response between ambient air and high-pressure oil conditions across all nine material configurations. TD and EQS consistently increase under oil submersion due to external pressure effects, with maximum EQS rise observed in L9-4 (+16.35 MPa). However, NS deltas exhibit high variability; for example, L9-4 experiences a reduction of over 30 MPa, highlighting the redistribution of loads under hydrostatic influence. These results emphasize the importance of evaluating mechanical behavior under dual environmental conditions to ensure robust, real-world flange coupling performance.

Trial	Δ Total Deformation (mm)	Δ Equivalent Stress (MPa)	Δ Shear Stress (MPa)	Δ Normal Stress (MPa)
L9-1	0.000384	4.02	6.9	22.97
L9-2	0.000924	6.19	3.04	–5.56
L9-3	0.001474	5.77	2.78	–5.45
L9-4	0.000839	16.35	7.23	–30.47
L9-5	0.000924	6.19	3.04	–5.56
L9-6	0.001474	5.77	2.78	–5.45
L9-7	0.000722	9.83	9.96	–5.54
L9-8	0.000924	6.19	3.04	–5.56
L9-9	0.001474	5.77	2.78	–5.45

TABLE 14: Sensitivity Comparison

Figure *13* illustrates the convergence behavior of the GA during fitness evolution, measured using CSPI, under two environmental scenarios. The curve labelled "Fitness (CSPI) Air" demonstrates a steady improvement in fitness across 100 generations, plateauing around a CSPI of 0.685. In contrast, the "Fitness (CSPI) Oil" curve shows a more gradual rise, stabilizing near 0.525. The reduced convergence slope and lower fitness ceiling in the oil condition reflect the added mechanical constraints and complexity induced by external hydrostatic pressure. The difference in final CSPI values highlights the GA's adaptability to changing environmental inputs and its ability to consistently find optimal trade-offs between mechanical reliability and sustainability criteria, in alignment with Industry 5.0 objectives.

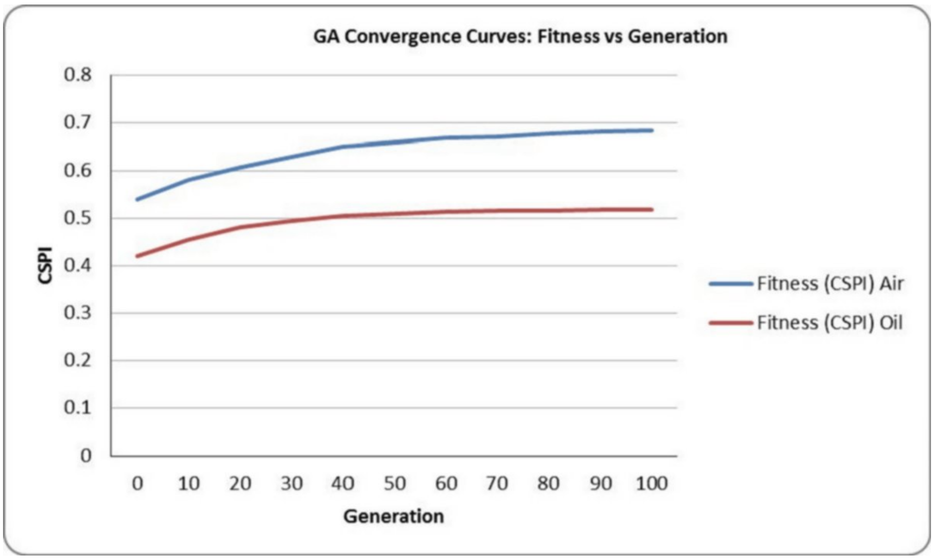

FIGURE 13: GA Convergence Curves: Fitness vs. Generation

GA, Genetic Algorithm

Conclusions

This study introduced a hybrid optimization framework for rigid flange coupling systems, integrating the Taguchi DOE, MCDM, and GA to identify optimal material configurations. The framework addressed both mechanical performance and environmental sustainability under realistic loading conditions, including high-pressure oil immersion scenarios.

Mechanical performance was assessed via finite element simulations of TD, EQS, SS, and NS. Parallelly, sustainability was evaluated using CF, ME, RI, and EoL impact metrics, normalized and sourced from industrial LCA databases. The methodology enabled a dual-objective trade-off, where the CSPI was used to rank each material combination under three weighting priorities: performance-dominant (α = 0.7), sustainability-dominant (α = 0.3), and balanced (α = 0.5). TOPSIS-based ranking identified L9-2 and L9-5 as consistently high-performing configurations across all α scenarios. The GA did not introduce a new optimal material configuration for the limited design space considered in this study; however, it successfully validated the Taguchi-TOPSIS outcome and demonstrated that the proposed hybrid framework is scalable, making it suitable for larger optimization spaces in future research. This confirms that the integrated approach is robust for balancing mechanical performance and sustainability across varying operating environments

Environmental robustness was validated through high-pressure oil simulations, which confirmed similar performance trends and stress distribution patterns. This demonstrates that the proposed optimization strategy is resilient and transferable across varied operating environments.

Overall, the hybrid optimization model provides a scalable, eco-efficient pathway for high-stress mechanical assemblies. By embedding sustainability into the material selection process and validating under dual environmental conditions, the framework aligns with Industry 5.0 design values-supporting future-ready, adaptive, and environmentally conscious engineering solutions.

Additional Information

Author Contributions

All authors have reviewed the final version to be published and agreed to be accountable for all aspects of the work.

Concept and design: Manoj M. Dongare, Swapnil S. Bhoir, Munna Verma

Acquisition, analysis, or interpretation of data: Manoj M. Dongare, Swapnil S. Bhoir, Munna Verma

Drafting of the manuscript: Manoj M. Dongare, Swapnil S. Bhoir, Munna Verma

Critical review of the manuscript for important intellectual content: Manoj M. Dongare, Swapnil S. Bhoir, Munna Verma

Supervision: Manoj M. Dongare, Swapnil S. Bhoir, Munna Verma

Disclosures

Human subjects: All authors have confirmed that this study did not involve human participants or tissue. **Animal subjects:** All authors have confirmed that this study did not involve animal subjects or tissue. **Conflicts of interest:** In compliance with the ICMJE uniform disclosure form, all authors declare the following: **Payment/services info:** All authors have declared that no financial support was received from any organization for the submitted work. **Financial relationships:** All authors have declared that they have no financial relationships at present or within the previous three years with any organizations that might have an interest in the submitted work. **Other relationships:** All authors have declared that there are no other relationships or activities that could appear to have influenced the submitted work.

References

1. Dongare MM, Bhoir SS, Verma M: Analysis and comparison of flange coupling models by using different materials in 3D printer. AIP Conference Proceedings. 2025, 020005. 10.1063/5.0234080
2. Dongare MM, Bhoir SS, Verma M: Integrating multi-criteria decision-making and the Taguchi method for high-performance material selection in rigid flange coupling systems. Cureus Journal of Engineering. 2025, 2:-. 10.7759/s44388-025-03722-w
3. Abushama K, Hawkins W, Pelecanos L, Ibell T: Optimising the embodied carbon of laterally loaded piles using a genetic algorithm and finite element simulation. Results in Engineering. 2024, 24:103188. 10.1016/j.rineng.2024.103188
4. Corriveau G, Guilbault R, Tahan A: Genetic algorithms and finite element coupling for mechanical optimization. Advances in Engineering Software. 2010, 41:422-26. 10.1016/j.advengsoft.2009.03.008
5. Feng X, Zhu X, Zhao W, Yan C: Coupling mechanical model and failure of aeroengine ceramic matrix composite based on genetic algorithm. Measurement: Sensors. 2024, 33:101226. 10.1016/j.measen.2024.101226
6. Huang H, He Q: Bolt looseness localization with connection-stiffness-varying flange. Smart Materials and Structures. 2024, 33:095005. 10.1088/1361-665x/ad6725
7. Imani V, Sevilla-Salcedo C, Moradi E, Fortino V, Tohka J: Multi-objective genetic algorithm for multi-view feature selection. Applied Soft Computing. 2024, 167:112332. 10.1016/j.asoc.2024.112332
8. Ji Y, Lu Q: A novel differential evolution algorithm for a flange coupling using ANSYS simulations. Frontiers in Materials. 2022, 9:10.3389/fmats.2022.1094596
9. Ke J, Li R, Lu W, Zhou H, Hu Y, Zhang J: Variable-stiffness mechanism investigation and optimization of SMA hybrid fabric composite leaf springs via an improved genetic algorithm. Materials Today Communications.

2025, 46:112873. 10.1016/j.mtcomm.2025.112873
10. Kuang Y, Peng S, Wang L, Chen L, Li W: Experimental investigation on the fatigue properties of studs under the coupling of load and corrosion environment. Materials and Structures. 2024, 57:237. 10.1617/s11527-024-02519-3
11. Li G, Nie Z, Zeng Y, Pan J, Guan Z: New simplified dynamic modeling method of bolted flange joints of launch vehicle. Journal of Vibration and Acoustics. 2020, 142:021011. 10.1115/1.4045919
12. Liu H, Sun W, Liu X, Ma H, Du D, Li H: Modeling and free vibration analysis of bolted composite flanged cylindrical-cylindrical shells under partial bolt loosening conditions. Thin-Walled Structures. 2024, 199:111853. 10.1016/j.tws.2024.111853
13. Liu X, Sun W, Liu H, Ma H, Du D, Li H: Generalized model for eigenfrequency analysis of bolted variable-stiffness flanged-cylindrical shells. International Journal of Mechanical Sciences. 2024, 282:109618. 10.1016/j.ijmecsci.2024.109618
14. Liu X, Sun W, Liu H, Ma H, Du D, Li H: Modeling and vibration analysis of bolted composite conical-conical shells with flanges. Thin-Walled Structures. 2024, 200:111955. 10.1016/j.tws.2024.111955
15. Lu X, Zeng Y, Chen Y, Xie X, Guan Z: Transient response characteristics of a bolted flange connection structure with shear pin/cone. Journal of Sound and Vibration. 2017, 395:240-57. 10.1016/j.jsv.2017.02.029
16. Luan Y, Guan ZQ, Cheng GD, Liu S: A simplified nonlinear dynamic model for the analysis of pipe structures with bolted flange joints. Journal of Sound and Vibration. 2012, 331:325-44. 10.1016/j.jsv.2011.09.002
17. Mao J, Wang W, Liu Y, Zhang J: Comparative study of flange-to-seal contact couplings with bolt relaxation under creep condition. Journal of Engineering for Gas Turbines and Power. 2014, 136:072504. 10.1115/1.4026656
18. Nancy M, Stephen EA: Modelling and analysis of the cone coupling problem using optimization. Mathematical Modelling of Engineering Problems. 2022, 9:1385-392. 10.18280/mmep.090529
19. Nurprasetio IP, Budiman BA, Triawan F: Failure investigation of plastic shredding machine's flange coupling based on mechanical analysis. Indonesian Journal of Science and Technology. 2017, 2:124. 10.17509/ijost.v2i2.7988
20. Shi W, Zhang Z: Elastostatic properties for flange-bolted joints. International Journal of Pressure Vessels and Piping. 2023, 205:104966. 10.1016/j.ijpvp.2023.104966
21. Wang L, Chen X, Fan Z, Xue J: FEM stress analysis of bolted flange joints in elevated temperature service condition. ASME 2018 Pressure Vessels and Piping Conference. 2018, 10.1115/PVP2018-84444
22. Xie M, Wei Z, Zhao J, Wang Y, Liang X, Pei X: Remaining useful life prediction of pipelines considering the crack coupling effect using genetic algorithm-back propagation neural network. Thin-Walled Structures. 2024, 204:112330. 10.1016/j.tws.2024.112330
23. Zahariea D: Structural analysis of a flange coupling without clearance. Applied Mechanics and Materials. 2013, 371:652-56. 10.4028/www.scientific.net/amm.371.652
24. Zou T, Liu W, Li M, Tao L: Fatigue assessment on reverse-balanced flange connections in offshore floating wind turbine towers. ASME 2021 40th International Conference on Ocean, Offshore and Arctic Engineering. 2021, 10.1115/OMAE2021-64973
25. Dongare M, Verma M, Bhoir S: Multi-response optimization of rigid flange coupling using Taguchi Design, ANOVA, and FEA in dual environmental conditions. Advanced Materials & Sustainable Manufacturing. 2025, 2:10011. 10.70322/amsm.2025.10011